https://doi.org/10.5194/egusphere-2025-6040
Preprint. Discussion started: 10 December 2025

Saltwater exposure accelerates ice grain growth and may increase fracture vulnerability

Authors: Cassandra Seltzer[1,2]*, Christine McCarthy[1], Andrew J. Cross[2], Michelle Berkmans[1,3], Noah Walls[4], Joanna D. Millstein[5]

Affiliations:

[1]Lamont-Doherty Earth Observatory, Columbia University; Nyack, USA.

[2]Woods Hole Oceanographic Institution; Woods Hole, USA.

[3]Kingsborough Community College; Brooklyn, USA.

[4]University of Southern California; Los Angeles, USA.

[5]Colorado School of Mines; Golden, USA.

*Corresponding author: cassandraseltzer@gmail.com

Abstract:

Natural ices often fail at stresses much lower than those measured in laboratory settings, complicating our understanding of glacial failure and icy moon crustal fracture. This may be because strength models, which depend on the size of individual ice grains, do not account for the saltwater commonly found in terrestrial and planetary ices. We conducted grain growth experiments, finding that saltwater always modifies grain growth compared to pure ice, and that increasing volume of saltwater introduces a pinning effect limiting this growth. Ice grain size therefore depends directly on liquid fraction, controlled by salinity and temperature. As such, we introduce an equation for grain growth parameters that is dependent on brine fraction and temperature relative to the liquidus. We then use our grain growth models to predict how saltwater infiltration affects ice strength. Modeled effects of grain growth on tensile strength following saltwater infiltration find that low-salinity water can reduce ice strength by up to 46% within 24 hours, narrowing gaps between observations and experiments.

https://doi.org/10.5194/egusphere-2025-6040
Preprint. Discussion started: 10 December 2025

1. Introduction

The strength evolution of icy materials is controlled by microstructural processes. Ice grain size, for example, is a crucial parameter for predicting future glacial mass balance (Alley, 1992; Alley et al., 1986; Behn et al., 2021; Faria et al., 2014a; Kingslake et al., 2022; Ranganathan & Minchew, 2024; Rignot et al., 2011) and the extent of heat released to maintain subsurface oceans in icy moons (Kihoulou et al., 2025; Nimmo, 2025; Nimmo & Manga, 2017; Poirier et al., 1983). As cryospheric environments like glaciers and icy moon interiors experience stress, they can deform both viscously and brittlely. It has been observed in laboratory settings that coarse-grained ices are more resistant to flow (Goldsby & Kohlstedt, 1997, 2001), yet also more susceptible to fracture (Currier & Schulson, 1982; Lee & Schulson, 1988; Schulson et al., 1984). Fracture yields macroscopic damage, such as crevassing and calving, that relieves buttressing stresses which otherwise resist fast glacial flow and mass loss at Earth's poles (Chudley et al., 2025), and allows faults or vents to propagate through the crusts of icy moons. Grain size evolution is therefore key to understanding the future of cryospheric environments. However, we do not yet have a good understanding of how grain growth proceeds if liquid water is present.

Grain size evolution in a single-phase material is commonly treated as a dynamic competition between processes that facilitate grain size reduction, such as dynamic recrystallization, and processes that drive normal or "static" grain growth driven by reduction of grain-boundary energy (Austin & Evans, 2007; Cross et al., 2015; De Bresser et al., 1998; Roessiger et al., 2011). Static grain growth is often modeled using an Arrhenius (or Hillert) relationship to predict grain size, d, as a function of time, t, such that

$$d(t)^p = d(t_0)^p + kt \quad \text{(Eq. 1)}$$

$$k = k_0 \exp(-Q/RT) \quad \text{(Eq. 2)}$$

where p is the grain-growth exponent, $d(t_0)$ is the initial grain size, k_0 is a constant, Q is activation enthalpy, R is the ideal gas constant, and T is temperature in Kelvin. The theoretical value of p (also called m or n in some literature) is 2 for pure, single-phase materials. For ice, p has been found to vary between 2 – 20 depending on the presence of bubbles, local conditions, and impurity content (Alley et al., 1986; Azuma et al., 2012; Faria et al., 2014a, 2014b; Jellinek & Gouda, 1969).

https://doi.org/10.5194/egusphere-2025-6040
Preprint. Discussion started: 10 December 2025

Laboratory studies show that below the eutectic temperature of a water-salt mixture, 251.95 K (−21.2˚C), where only solid phases are present, grain growth is inhibited relative to pure ice (De Achaval et al., 1987; Jellinek & Gouda, 1969; Wang et al., 2024). This is because impurities preferentially segregate to grain boundaries, where they exert drag and reduce boundary mobility by orders of magnitude (Gleiter, 1969). Conversely, at temperatures above the minimum eutectic temperature of a water-salt mixture where saline water is present between grains (the concentration of which is determined by relative distance from a liquidus curve; Figure S1), grain growth is *enhanced* by the presence of salts (De Achaval et al., 1987; Jellinek & Gouda, 1969). This observation is often attributed to the fact that diffusion is energetically easier through an interstitial liquid phase than along a solid-solid interface (e.g., Cooper & Kohlstedt, 1984). However, the influence of salinity and liquid fraction have not been determined in isolation; it is not yet clear whether grain growth enhancement in the presence of a brine is due to the presence of the liquid alone, or if the salinity and volume of liquid further affect grain growth.

To address uncertainty relating temperature, salinity, and grain size, we conducted static grain-growth experiments on ice of varying salinities at temperatures above the H_2O-NaCl eutectic minimum. We characterized grain sizes and dihedral angles through microstructural imaging and hand tracing. In doing so, we found that grain growth was always higher in salty ice than in pure ice. However, we also found that increasing salinity, and therefore an increasing amount of saltwater, inhibited grain growth. We provide a physical explanation for this observation, establish a constitutive relationship for grain growth parameters as a function of both salinity and temperature, and discuss the implications for ice dynamics in cases of tensile failure.

2. Methods

We surveyed a range of salinities and temperatures in order to explore different melt fractions in the NaCl-H_2O eutectic system (Figure 1A). By holding salinity or temperature constant, we were able to explore variations in melt fraction and the “vertical lever” (Figure 1B), a quantity which has been shown to simplify variations between systems in properties like acoustic velocities (McCarthy et al., 2019).

https://doi.org/10.5194/egusphere-2025-6040
Preprint. Discussion started: 10 December 2025

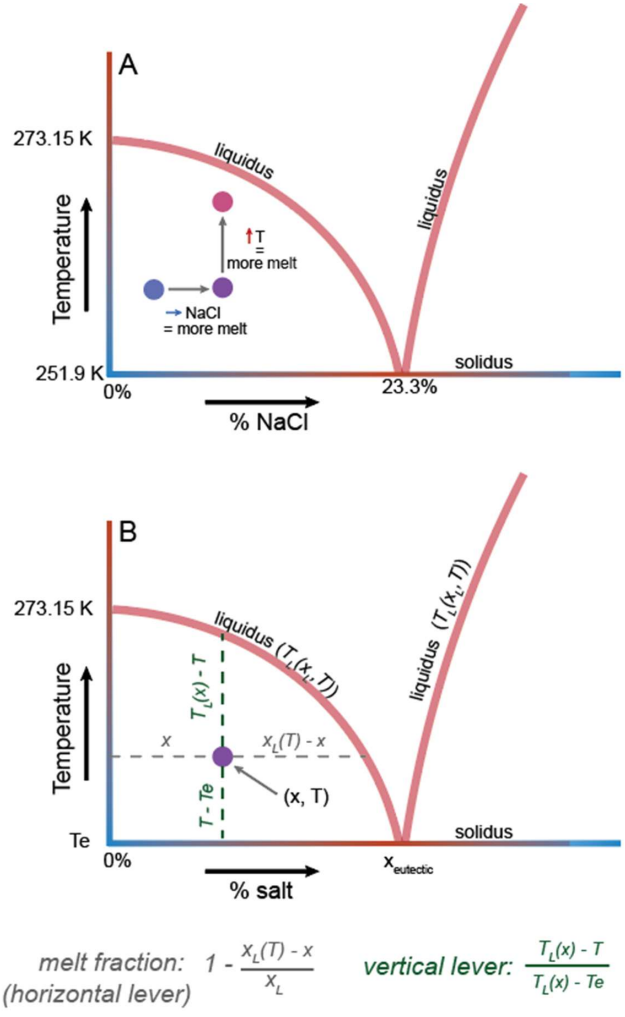

Fig. 1. Eutectic diagrams in a saline-H2O system. A) Diagram specific to the NaCl-H_2O system, showing how increasing temperature and increasing salinity both add more melt by drawing a salty ice aggregate closer to the liquidus curve. B) Generic eutectic diagram indicating the calculation of melt fraction and the "vertical lever."

2.1 Sample Fabrication

Individual ice samples with "high" salinity (HS), "low" salinity (LS), and no salinity (NS) were prepared using the freeze-flood "standard ice" method of (Cole, 1979), adapted for eutectic mixtures as described by Ravikumar et al. (2025). First, bubble-free ice made from pure, deionized water was ground and sieved to obtain ice particles of 106–250 μm diameter. This ice powder was packed into a die with internal dimensions of 50.8 × 50.8 × 19.8 mm, which was sealed with vacuum grease, and placed in a saltwater

https://doi.org/10.5194/egusphere-2025-6040
Preprint. Discussion started: 10 December 2025

bath at 268 K (HS/LS) or 272 K (NS) or below. This temperature exposure does not cause ice grains to grow, as the die preserves the temperature of 259 K or below used in the freezer during preparation. The die was then placed under a vacuum relative pressure of −0.98 bar for at least 30 minutes to remove any pore space between ice particles. Next, the die was flooded with either saline water of 5 wt.% (HS) or 2.9 wt.% (LS) NaCl, or pure deionized water (NS). Vacuum was maintained until this "flood" water percolated through the entire sample, at which point the sample was promptly disconnected from vacuum, and placed on a copper plate in a chest freezer at 248 K for at least 12 hours to initiate unidirectional, bottom-up freezing expelling any trapped air.

To characterize the initial microstructures, a flat surface of each sample was prepared via cryomicrotome, then imaged using a reflected-light microscope in a walk-in freezer at temperatures below the minimum H_2O-NaCl eutectic temperature (251.8 K). Grains within the NS samples grew tightly packed during freezing, and so had slightly larger initial grain sizes than the HS/LS samples. Pieces of each sample were also collected for analysis of their salinity using a handheld refractive-index meter and the calibration curves (Ravikumar et al., 2025). The effective bulk salinities of the HS samples fell between 1.31–2.17 wt% NaCl, the salinities of LS samples fell between 0.34–0.74 wt% NaCl, and the NS samples had 0 wt% NaCl (or other impurities). For context, natural sea ices cover a similar range of salinities, up to 3.5% (Weeks, 2010).

2.2 Grain growth procedure

Each sample was cut into rectangular pieces of 16.9 × 50.8 × 19.8 mm, and vacuum sealed in plastic bags. Experiments were named by the convention xSyT, where x was H/L/N to indicate salinity, and y was H/L to indicate high/low temperature (268 K and 260 K, respectively), followed by a number (1/2) to indicate the sample prep number (from the first or second batch of samples) and a letter (A/B/C/D/E) to indicate the duration of annealing at the given temp (3.16hr/7hr/31hr/100hr/316hr). For example, sample LSHT2.E was a low-salinity sample annealed at relatively high temperature, came from the second batch of LSHT samples, and was annealed for 316 hours. Samples were placed in an insulated box inside each freezer that stabilized temperatures by reducing the duty cycle effect (Figure S1). After annealing, samples were quenched using liquid nitrogen to capture the microstructure at the exact time of removal, and then stored in a freezer at 218 K for at least two hours.

2.3 Imaging and analysis

Each sample was microtomed in a freezer below 251.8K, then imaged in reflected light microscopy. Refractive indices were measured at this point as well to compare with the starting material so as to confirm that no leaking or contamination had occurred during annealing or processing. Grains in each

https://doi.org/10.5194/egusphere-2025-6040
Preprint. Discussion started: 10 December 2025

image were then hand-traced and converted to equivalent mean diameter. In several samples, two perpendicular sides were polished in order to verify that no columnar growth occurred and that the assumption of roughly spherical particles was appropriate (Fig S2). We also took images of selected samples after one month in the 218K freezer, to ensure that no further grain growth happened while samples were in storage (Fig S2F). Grain size was then measured by hand-tracing reflected-light images, converting shapes to pixel area, and calculating the mean grain diameter for area-equivalent circles. We report arithmetic mean grain sizes (diameters) for consistency with previous studies of grain growth in saline ice (De Achaval et al., 1987; Wang et al., 2024).

Dihedral angles were also hand-traced and measured using reflected-light images following methodology described by (McCarthy et al., 2019) (Fig S3). The dihedral angle provides an indicator of melt network connectivity. For instance, at dihedral angles greater > 60°, interconnected melt networks will not form and melt will, instead, be confined to isolated pockets at grain junctions (Bulau et al., 1979).

3. Results

3.1 Grain growth

Grain boundaries traced from high-salt (HS) and low-salt (LS) samples are shown in Figure 2. In both the high-temperature (HT) and low-temperatures (LT) experiments, grain boundaries became slightly straighter, while small grains were consumed by larger grains over time (Figures 2A–F, S4).

https://doi.org/10.5194/egusphere-2025-6040
Preprint. Discussion started: 10 December 2025

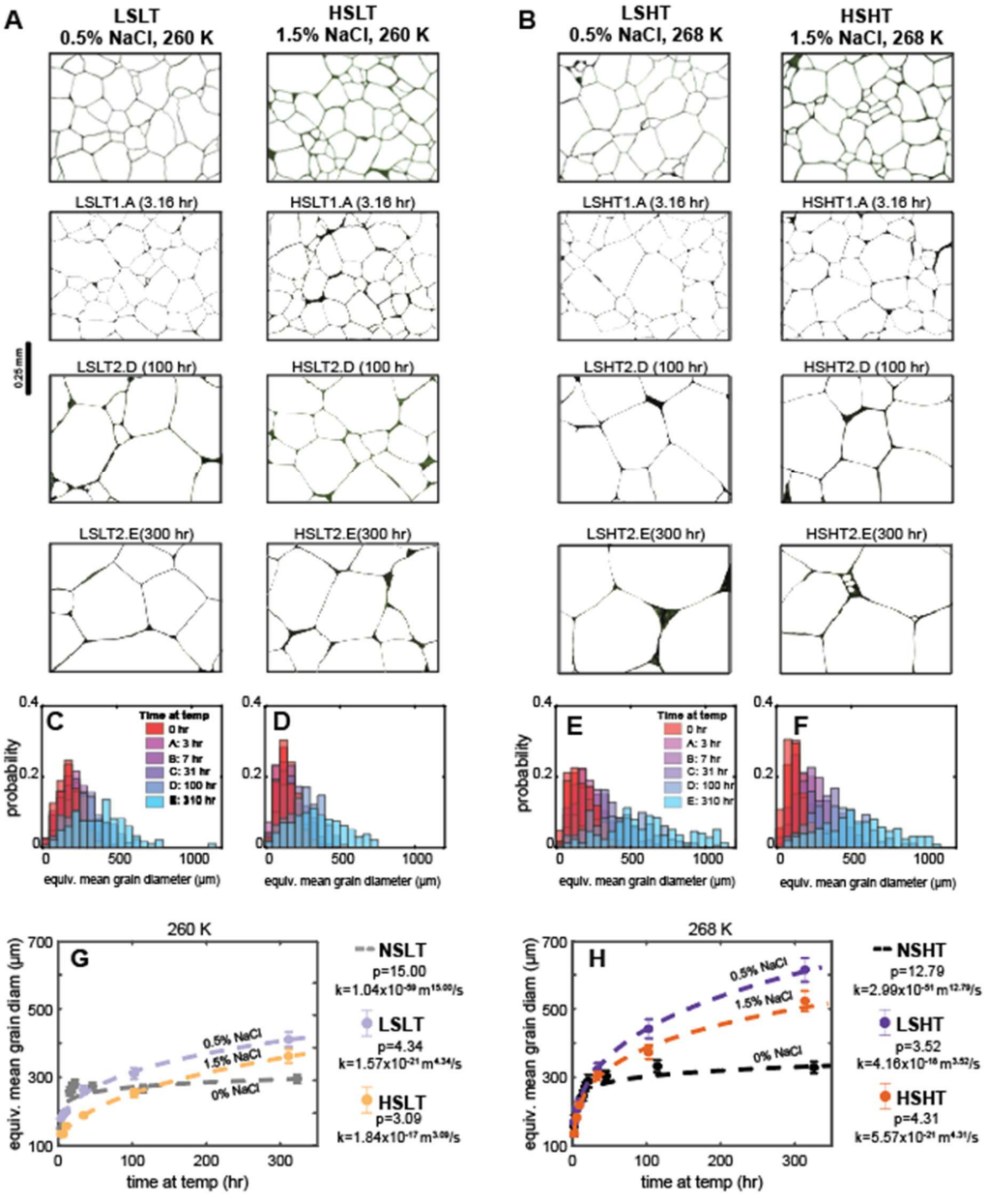

Fig. 2. Grain sizes from growth experiments on ice after saltwater exposure. Traced grain outlines from low-temperature (**A**) and high-temperature (**B**) grain growth tests, labeled by the duration of tests and the salinity. Top row of all images shows grain boundaries from starting material. Additional tracings can be found in Figure S1. Histograms (**C – F**) and grain law fits (**G – H**) show that the population of larger grains increases with time, and that the shape of the distribution across samples remains somewhat constant as a function of temperature. Lower-salinity

https://doi.org/10.5194/egusphere-2025-6040
Preprint. Discussion started: 10 December 2025

grains also consistently grow larger than higher-salinity grains at the same given temperature, and both exceed the growth rate of salt-free ice.

https://doi.org/10.5194/egusphere-2025-6040
Preprint. Discussion started: 10 December 2025

All experiments shown here are well fit by the standard equation for grain growth (Eq 1; Figure 2E – F; Table S1). We used least-squares regression to derive the best-fit values of the grain-growth exponent, p (limited to values between 0 and 20), and grain-growth constant, k, in each example. In agreement with (Wang et al., 2024) we find that p = 3–4.5 provides the best fit, and that there is no clear relationship between salinity, temperature, and the value of p. This finding also agrees with observations, from silicates, that grain growth in the presence of extrinsic drag forces will have a value of $p > 2.5$ (Evans & Dresen, 1991); higher than the commonly cited $p = 2$ for idealized, single-material grain growth. For ease of comparison with earlier results, we normalized to $p = 4$. We observe that k-values, once normalized to growth exponent of $p = 4$, fall within the range of $1 – 10 \times 10^{-20}$, while those for pure ice at the same temperatures are an order of magnitude lower. Grain growth was thus usually much slower in pure ice samples than in any salt-and-melt-bearing sample at the same temperature (Figure 2G – H, Figure S4, Figure S5); however, p-values were much higher, indicating a quick plateau in grain growth. Furthermore, we note that grain size distribution moves from a lognormal to a more symmetric, normal distribution once grain growth begins to plateau (Figure 2C – F).

The presence of melt therefore modifies grain growth compared to pure ice at a given temperature, but higher salinities limit growth compared to lower salinities. This is sensible in the context of previous findings that salinity impedes crystal growth *below* the eutectic temperature (De Achaval et al., 1987; Jellinek & Gouda, 1969; Wang et al., 2024). Previous experimental work also noted that above the eutectic point in the NaCl-H_2O and KCl-H_2O systems, grain growth is faster than that of pure ice at the same temperature (Chatterjee & Jellinek, 1971; Jellinek & Gouda, 1969; Wang et al., 2024). A closer inspection of results by Wang et al., (Wang et al., 2024) who did not draw conclusions regarding the effects of salinity on grain growth above the eutectic, also shows that grain growth above the eutectic temperature is faster than in samples with a KCl concentration of 10^{-5} M than those with 10^{-2} M KCl (Figure 3). This agrees well with our results, as well as the increased grain boundary mobility inverse to KCl concentration seen by (Nasello et al., 2007).

https://doi.org/10.5194/egusphere-2025-6040
Preprint. Discussion started: 10 December 2025

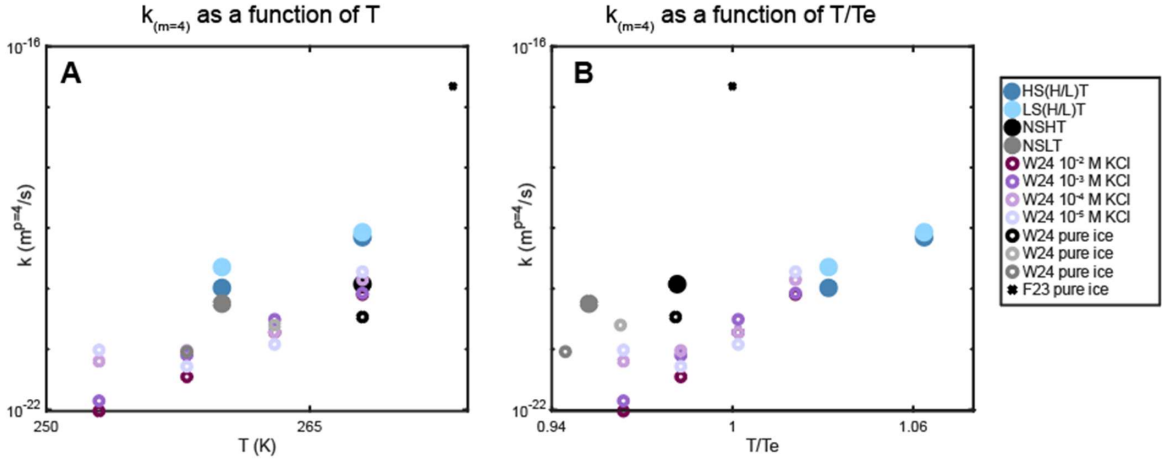

Fig. 3.
Values of grain growth parameter k (for a fixed $p = 4$) for chloride salts mixed with H_2O ice as a function of (**A**) absolute temperature, and (**B**) temperature relative to the eutectic temperature, using values from this study and Wang et al (2024), W24, and pure ice to the eutectic temperature from Fan et al (2023), F23. The relationship between salinity and k is not straightforward very close to the eutectic temperature, but below 0.96 T/Te and above 1.03 T/Te, higher-salinity samples have lower k values.

3.2 Dihedral angles

Dihedral angles varied modestly as a function of both salinity and temperature (Fig 4). The LS experiments uniformly showed higher dihedral angles than HS experiments, with melt tending to form between grains at triple junctions in LS experiments (Figures 4A – B), while HS experiments showed long melt veins between grains throughout.

All values of θ were below 60°, suggesting that saltwater within icy aggregates will nearly always form an interconnected melt network (Bulau et al., 1979). Dihedral angle also did not evolve appreciably with time in the LT (−13°C) experiments (Figures 4C–D, 4G) but did decrease significantly with time in the HT (−5°C) experiments (Figures 4E–F, 4H), where for both concentrations the θ values flatten to ~14°. The decrease in θ with saltwater exposure time agrees with previous observations that grain growth may preferentially remove high-energy grain boundaries, and therefore higher dihedral angles (Xu et al., 2023).

https://doi.org/10.5194/egusphere-2025-6040
Preprint. Discussion started: 10 December 2025

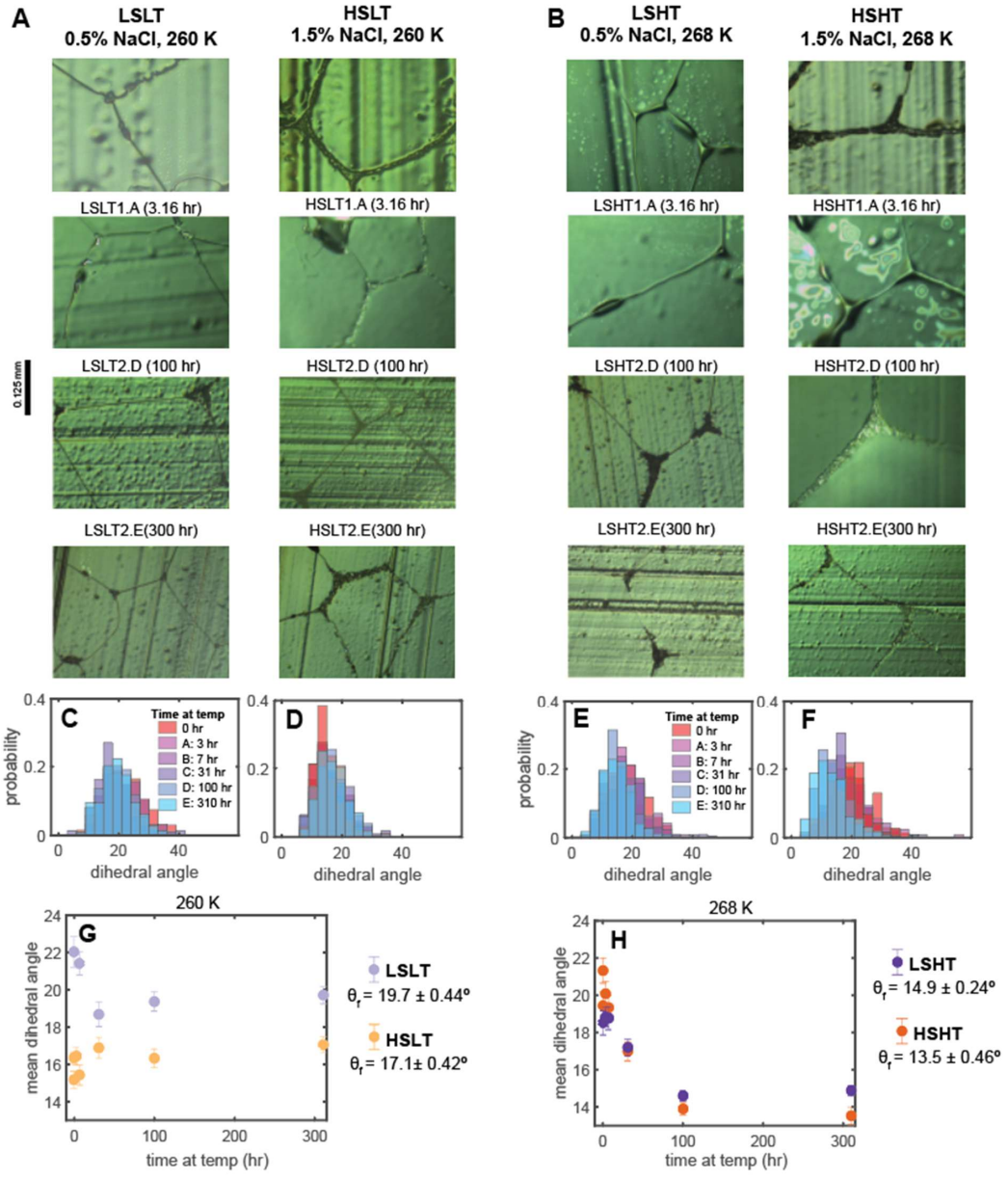

220 **Fig. 4.** Dihedral angles. Traced dihedral angles from low-temperature (**A**) and high-temperature (**B**) tests show that lower-salinity samples host liquid primarily at triple junctions, while higher-salinity samples host liquid along grain boundaries throughout. Top row of all images is the dihedral angle from starting material. Histograms (**C – F**) and plots of mean dihedral angle as a

https://doi.org/10.5194/egusphere-2025-6040
Preprint. Discussion started: 10 December 2025

function of time (**G – H**) show that lower-temperature dihedral angles remain roughly constant, while higher-temperature samples tend to decrease their dihedral angle with grain growth.

4. Discussion

We note that higher grain sizes are found in the lowest-salinity aggregates at both temperatures observed, such that an increased brine fraction limits grain growth. We suggest that increased saltwater therefore creates a pinning effect, which may lead to smaller grains and therefore change the effective strength of icy material.

4.1 Pinning effects of saltwater on grain growth

The extrinsic drag forces that limit grain growth at melt-grain interfaces can be modeled as a form of Zener pinning (see (Alley et al., 1986), wherein the surficial energy of a melt pocket exerts a limiting force on grain growth.

The interfacial energy between solid and liquid phases (γ_{SL}), and the interfacial energy between solid and solid phases (γ_{SS}, approximately 0.065 mJ/m^2; (Ketcham & Hobbs, 1969), are related by dihedral angle at a liquid-solid interface, θ, (Figure S5) such that

$$\gamma_{SL} = \frac{\gamma_{SS}}{2\cos\left(\frac{\theta}{2}\right)}$$

(Eq. 3)

Pinning pressure is then expressed as

$$P_z = \frac{3f\,\gamma_{SL}}{2r_p}\psi$$

(Eq. 4)

where γ_{SL} is the grain-boundary energy at a solid-liquid interface, r_p is the radius of the melt pocket, and ψ is a shape correction term to modify the deviation from assumed spherical particles. This has units of J/m^3, equivalent to Pascals. The dihedral angle θ is also closely associated with changes to geophysical properties like seismic velocities (Hier-Majumder & Abbott, 2010), crystallization history (Holness et al., 2005, 2012), and short-term anelastic energy dissipation (Yamauchi et al., 2024; Yamauchi & Takei, 2024).

https://doi.org/10.5194/egusphere-2025-6040
Preprint. Discussion started: 10 December 2025

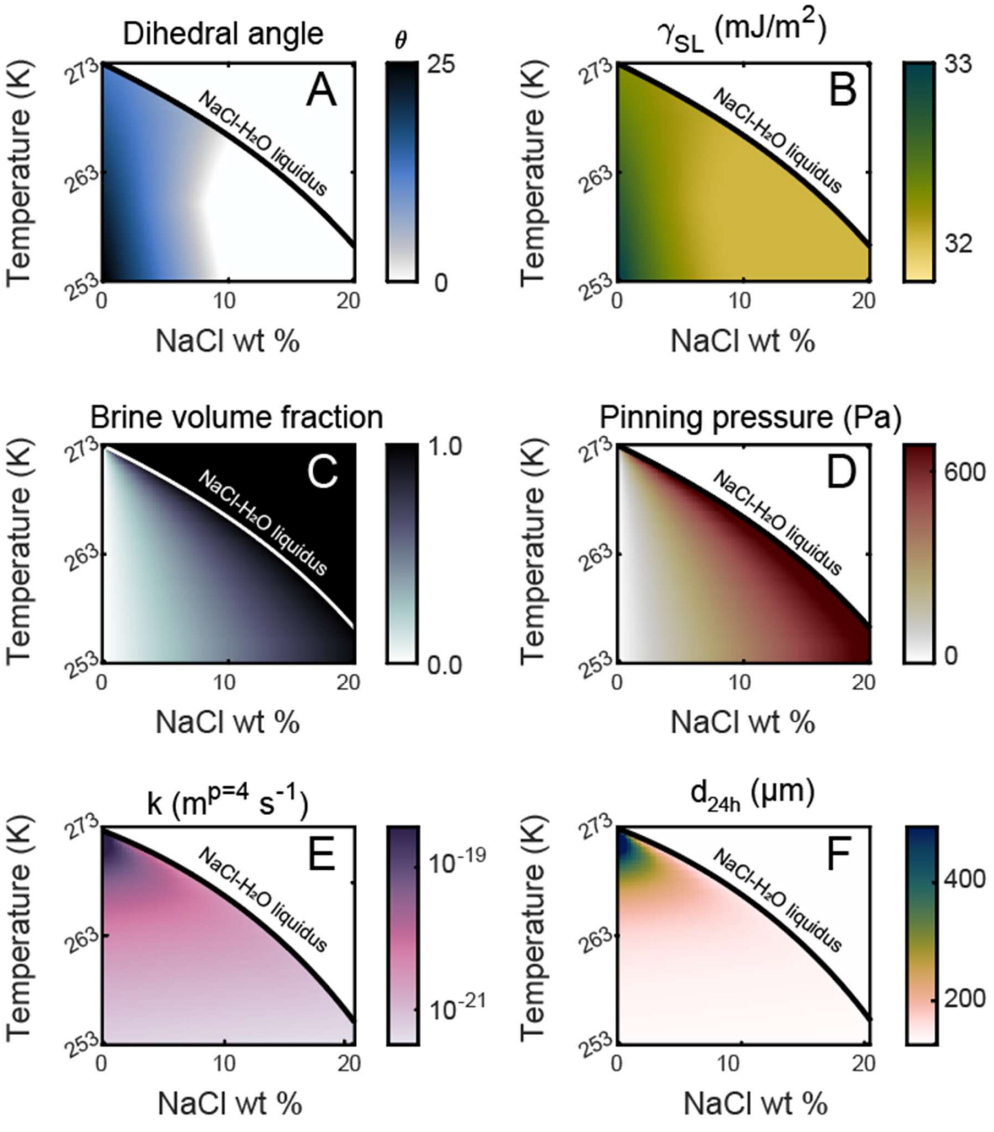

Fig. 5. Pinning calculations up to the NaCl-H_2O eutectic melting curve. (**A**) Dihedral angle extrapolated from experimental range of dihedral angles. Dihedral angles are always low enough to ensure connectivity, and above ~8 wt% NaCl, the dihedral angle falls close to 0, at which point all grain boundaries are fully lubricated. (**B**) γ_{SL}, surface energy at solid-liquid interfaces. Higher energy allows for enhanced grain growth. (**C**) Brine volume fraction as a function of temperature and NaCl wt %. (**D**) Zener pinning pressure of a saline water particle with radius of 50

https://doi.org/10.5194/egusphere-2025-6040
Preprint. Discussion started: 10 December 2025

μm. (**E**) Extrapolated *k* values for chloride salts as a function of weight percentage, temperature, and eutectic
265 temperature, using a fixed $p = 4$. (**F**) Projected grain size after 24 hours for a grain of initial diameter d = 150μm.

https://doi.org/10.5194/egusphere-2025-6040
Preprint. Discussion started: 10 December 2025

4.1.1 Grain growth parameters as a function of salinity and temperature

To explore all possible effects of saltwater on grain growth, we linearly interpolated dihedral angles in salinity-temperature space up to the NaCl-H_2O eutectic curve (Figure 5A) to calculate γ_{SL} (Eq. 3, Figure 5B), then used the lever rule to calculate effective melt fraction as a function of salinity and temperature (Figure 5C). We then calculated the effective local pinning pressure per unit micron of grain boundary (Eq. 4, Figure 5D). Pinning pressures generally increase with salinity such that, for a given temperature, lower salinities exhibit lower pinning pressure and therefore enhance grain growth compared to higher salinities.

We also parameterized k for impure ice (k_{im}) as a function of both composition and temperature relative to the eutectic point. We compiled k values for a fixed grain growth exponent of $p = 4$ from this study, as well as previously reported values in the KCl-H_2O and $MgSO_4$-H_2O systems (Wang et al., 2024). We build from the 'vertical lever rule' (McCarthy et al., 2019), which relates the temperature, minimum eutectic temperature, and liquidus by

$$V_L(x, T, Te) = \frac{T_L(x) - T}{T - Te} \quad \text{(Eq. 5)},$$

where x is chloride salinity as a weight fraction, $T_L(x)$ is the liquidus temperature at a given composition (see Supporting Information; Fig S1B), T is temperature in Kelvin, and Te is the eutectic temperature of a chloride system in Kelvin.

In doing so, we found that k_{im} can be calculated as a function of melt fraction (fm), V_L, and T, as

$$k_{im}(f_M, V_L, T) = \exp(\, A * (1 - f_M) \; * \; (V_L + 1)^B \,) * k_{pure} * \exp\left(-\frac{Q}{RT}\right) \quad \text{(Eq. 6)},$$

where $k_{0_{pure}}$ is 6.19 x 10^{-8} m^4/s and Q is 68 ± 47 kJ, following (Wang et al., 2024)

Using a nonlinear least-squares regression for compiled k-values across systems, we find that A = 8.209 ± 0.001 and B = -4.75 ± 0.41 (Figure S6).

https://doi.org/10.5194/egusphere-2025-6040
Preprint. Discussion started: 10 December 2025

300

4.1.2 Grain growth as a function of salinity and temperature

Using Eq. 6, we substitute k_{im} as k in Eq. 1 to calculate theoretical grain size after 24 hours (Figure 5F) in a new setting (i.e., 24 hours of melt exposure if above the eutectic temperature) using an initial d = 150 μm. This shows that grain size is indeed highly dependent on salinity and temperature relative to the eutectic temperature, and therefore the melt fraction. As seen in previous grain-growth studies, grain growth becomes considerably faster in the presence of liquid.

Using a modeled p = 4 matched results from a recent test on the grain-size-sensitive deformation of temperate ice with small degrees of meltwater present (Schohn et al., 2025), but only when ks are higher than those observed in saline systems (on the order of 10^{-16} – 10^{-14}; Figure S7). This agrees well with our finding that increased salinity can create a pinning pressure above the eutectic point, and points to the need for increased understanding of grain growth close to 273.15 K.

4.2 Implications for tensile strength of natural ice

Our finding that salinity and melt control the grain growth of temperate ice provides important insight into the physical properties of terrestrial and planetary cryospheres. For example, there is an orders-of-magnitude difference between measured laboratory strength (Currier & Schulson, 1982; Lee & Schulson, 1988; Litwin et al., 2012; Petrovic, 2003) and inferred natural strength from field observations (Grinsted et al., 2024; Ultee et al., 2020; Vaughan, 1993; Wells-Moran et al., 2025) of temperate ice. We follow the methodology of (Ranganathan & Robel, 2025) to model the dependence of tensile strength, σ_t on grain size, following the relationship

$$\sigma_t = K\, d^{-\frac{1}{2}} + \sigma_0 \quad \text{(Eq. 7)}$$

Where K and σ_0 are free parameters representing linear grain size dependence and theoretical initial tensile strength at a grain size approaching 0, and d is grain size in meters. We considered the relationship between a pure-ice mass of an ambient temperature, then model grain size as a function of time using modeled k_{im} (Figure 3E), using K = 0.052 MPa$^{1/2}$ and σ_0 = 0.5165 (Ranganathan & Robel, 2025). The choice of K did not significantly change the modeled tensile strength of our experiments (Figure S8). This model simulates settings in which either salty water infiltrates through grain boundaries in ice masses, as has recently been shown to increase fracture susceptibility in glaciers (Chen et al., 2025) and is likely in icy moons containing interstitial brines, or where impure ice experiences warming.

https://doi.org/10.5194/egusphere-2025-6040
Preprint. Discussion started: 10 December 2025

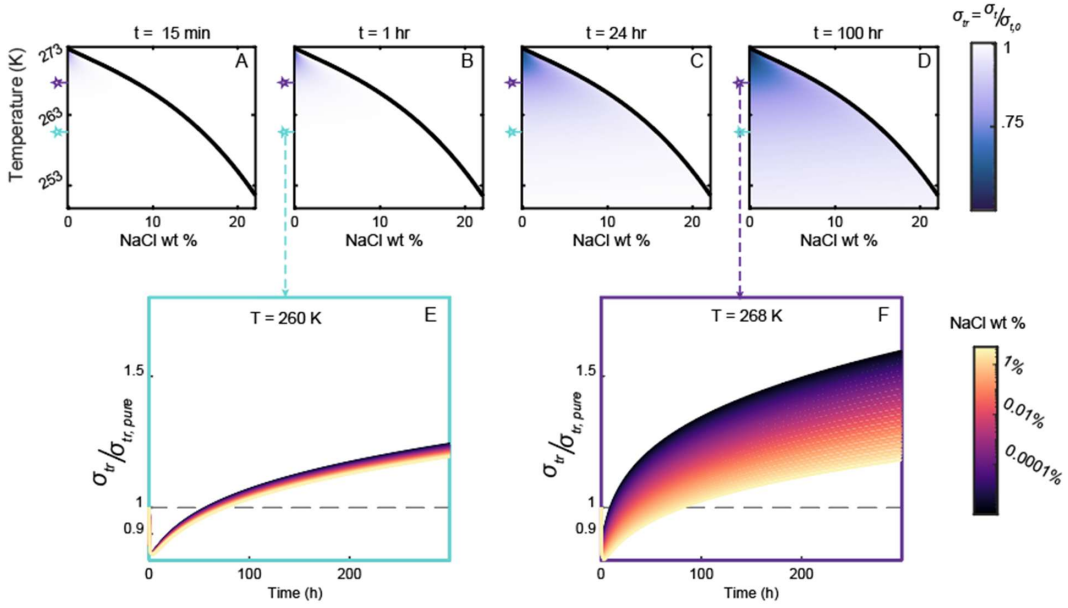

335 **Fig. 6.** Effective tensile strength of ices exposed to salty water, (**A – D**), as a percentage of initial tensile strength $\sigma_{t,0}$, over a period of (**A**) 15 minutes, (**B**) 1 hour, (**C**) 24 hours, and (**D**) 100 hours, as well as relative to the reduction in tensile strength due to temperature increases alone (normalized to 1 and indicated with a dashed line) in pure ice over the same periods at (**E**) 260 K and (**F**) 268 K, colored by NaCl weight percentage.

340

Saltwater significantly reduces the tensile strength of an icy aggregate in all cases, and lower-salinity infiltration yields the largest decreases in strength (Figure 6; Figure S8). Given a moderate initial tensile strength and 0.25% bulk salinity, these decreases can be up to 22.06 ± 0.06% after just one hour of saltwater exposure, and up to 40.76 ± 0.04% after 24 hours. If the salinity increases to 1%, the limiting
345 effect of melt on grain growth caps this tensile strength reduction at 7.99 ± 0.05% in the first hour and 28.32 ± 0.06% after 24 hours. Modeled tensile strength reductions in ice exposed to heat, but not saltwater, are initially higher than those from ice exposed to saltwater (Figure 6E – F), but lower-salinity saltwater can match the effects of temperature alone within 12 hours, and cause reductions in tensile strength up to 1.67 times that of temperature alone. Models of tensile strength based on saltwater
350 infiltration should thus predict a buttressing effect over hourslong timescales (relative to decreases from heat alone) that depends on the amount of saltwater present, but increasingly weaker ice masses with time.

Our results contribute to growing observational evidence that rheological and compositional
355 differences in glacier ice impede or impel failure (Borstad et al., 2017; King et al., 2018; Kulessa et al.,

https://doi.org/10.5194/egusphere-2025-6040
Preprint. Discussion started: 10 December 2025

2019), and that liquid infiltration can cause severe ice shelf instability (Suganuma et al., 2025). Furthermore, the presence of subsurface brine sills like those hypothesized to exist on Europa (Barr & Showman, 2009; Chivers et al., 2023; Steinbrügge et al., 2020; Wolfenbarger et al., 2022) means that interiors of icy moon cryospheres are likely weaker than expected, explaining features like putative cryovolcanic vents and fracture surfaces. The co-evolution of grain size and dihedral angle together also suggest that most of the short-term energy dissipation seen as icy moons orbit their host planets will occur within 100 Earth hours of enhanced saltwater infiltration, as reduced dihedral angles and slowed grain growth indicate lower grain boundary energy. As saltwater infiltrates into icy crusts, melt networks can form and reduce local strengths and viscosities, leading to enhanced grain growth in regions of infiltration. Further study is required to understand the competition between grain growth and melt lubrication in determining the viscosity of ice after saltwater infiltration.

5 Conclusions

We find that the grain size and dihedral angle, two key parameters for interpreting the microstructural behavior of partially molten icy aggregates, are modified significantly in the presence of saltwater. While any amount of saltwater changes the rate of grain growth and therefore grain size compared to pure ice, we find that increased salinity of an aggregate can reduce grain size and dihedral angle compared to lower salinities at the same temperature. We also observed that elevated temperature may further reduce dihedral angles in both higher and lower salinity ice aggregates. Our results also agree with recent experimental studies showing that a grain growth exponent of $p \sim 4$ may be more appropriate for salty aggregates than the commonly used values of $p = 2$ for pure ice or $p > 6$ for bubbly ice. We also established a relationship of grain growth parameter k that depends on both salinity and temperature for chloride salts mixed with ice.

The limiting effect of increasing salinity and saltwater volume fraction is well explained by the physics of grain pinning, and can be extrapolated over a wide range of temperature-salinity conditions to better predict the dynamics of ice in contact with saltwater or containing saline inclusions.

We show that the presence of saltwater can induce a much stronger reduction in tensile strength compared to the effects of temperature alone, and that increasing salinity enhances this effect. Preliminary results show that grain growth in the presence of saltwater may reconcile orders-of-magnitude differences in tensile strength between lab and natural settings. Our finding that saltwater weakens icy aggregates by enhancing grain growth, but that increased salinity may suppress grain growth, suggests that future studies coupling local salinity and temperature gradients could be strong predictors of glacial mass loss.

https://doi.org/10.5194/egusphere-2025-6040
Preprint. Discussion started: 10 December 2025

Acknowledgments: We thank Meghana Ranganathan and Elvira Mulyukova for discussions on existing data and implications of grain growth in the presence of melt, as well as Matěj Peč and Abhishek Prakash for conversations about grain growth in silicate systems. We would also like to thank Charlotte Bate, Maheenuz Zaman, and Caitlin Huntsman for assistance with sample fabrication and grain tracing.

Funding:

National Science Foundation grant NSF-OPP 2420207 (CS)

National Science Foundation grant NSF-EAR-2349621 (Lamont-Doherty Earth Observatory)

Author contribution:

Conceptualization: CS

Methodology: CS, CM

Investigation: CS, MB, NW

Validation: CS, MB

Writing – original draft: CS, CM, AJC, JM

Formal analysis: CS, MB

Supervision: CS, CM, AJC

Competing interests: Authors declare that they have no competing interests.

Code/data availability: A MATLAB structure storing all images and processed data used in this work, along with a sample script for processing grain means and pinning pressures are available at (Seltzer, 2025). Physical samples are stored at Lamont-Doherty Earth Observatory and may be accessed on request.

Supplementary Materials

Supplementary Text

Figs. S1 to S8

Table S1

https://doi.org/10.5194/egusphere-2025-6040
Preprint. Discussion started: 10 December 2025

References and Notes

Alley, R. B. (1992). Flow-law hypotheses for ice-sheet modeling. *Journal of Glaciology*, *38*(129), 245–256. https://doi.org/10.3189/S0022143000003658

Alley, R. B., Perepezko, J. H., & Bentley, C. R. (1986). Grain Growth in Polar Ice: I. Theory. *Journal of Glaciology*, *32*(112), 415–424. https://doi.org/10.3189/S0022143000012120

Austin, N. J., & Evans, B. (2007). Paleowattmeters: A scaling relation for dynamically recrystallized grain size. *Geology*, *35*(4), 343–346. https://doi.org/10.1130/G23244A.1

Azuma, N., Miyakoshi, T., Yokoyama, S., & Takata, M. (2012). Impeding effect of air bubbles on normal grain growth of ice. *Journal of Structural Geology*, *42*, 184–193. https://doi.org/10.1016/j.jsg.2012.05.005

Barr, A. C., & Showman, A. P. (2009). Heat Transfer in Europa's Icy Shell. In *Europa* (p. 405). https://ui.adsabs.harvard.edu/abs/2009euro.book..405B

Behn, M. D., Goldsby, D. L., & Hirth, G. (2021). The role of grain size evolution in the rheology of ice: Implications for reconciling laboratory creep data and the Glen flow law. *The Cryosphere*, *15*(9), 4589–4605. https://doi.org/10.5194/tc-15-4589-2021

Borstad, C., McGrath, D., & Pope, A. (2017). Fracture propagation and stability of ice shelves governed by ice shelf heterogeneity. *Geophysical Research Letters*, *44*(9), 4186–4194. https://doi.org/10.1002/2017GL072648

Bulau, J. R., Waff, H. S., & Tyburczy, J. A. (1979). Mechanical and thermodynamic constraints on fluid distribution in partial melts. *Journal of Geophysical Research: Solid Earth*, *84*(B11), 6102–6108. https://doi.org/10.1029/JB084iB11p06102

Chatterjee, A. K., & Jellinek, H. H. G. (1971). Calculation of Grain-Boundary Thickness in Polycrystalline Ice of Low Salinity. *Journal of Glaciology*, *10*(59), 293–297. https://doi.org/10.3189/S0022143000013253

Chen, H., Rignot, E., Scheuchl, B., Milillo, P., Morlighem, M., Gadi, R., Ciracì, E., Kim, J. H., & Dini, L. (2025). Rapid retreat of Berry Glacier, West Antarctica, linked to seawater intrusions revealed by radar interferometry. *Nature Communications*, *16*(1), 9292. https://doi.org/10.1038/s41467-025-64330-0

Chivers, C. J., Buffo, J. J., & Schmidt, B. E. (2023). Stable Brine Layers beneath Europa's Chaos. *The Planetary Science Journal*, *4*(9), 159. https://doi.org/10.3847/PSJ/acea75

Chudley, T. R., Howat, I. M., King, M. D., & MacKie, E. J. (2025). Increased crevassing across accelerating Greenland Ice Sheet margins. *Nature Geoscience*, *18*(2), 148–153. https://doi.org/10.1038/s41561-024-01636-6

https://doi.org/10.5194/egusphere-2025-6040
Preprint. Discussion started: 10 December 2025

Cole, D. M. (1979). Preparation of polycrystalline ice specimens for laboratory experiments. *Cold Regions Science and Technology*, *1*(2), 153–159. https://doi.org/10.1016/0165-232X(79)90007-7

Cross, A. J., Ellis, S., & Prior, D. J. (2015). A phenomenological numerical approach for investigating grain size evolution in ductiley deforming rocks. *Journal of Structural Geology*, *76*, 22–34. https://doi.org/10.1016/j.jsg.2015.04.001

Currier, J. H., & Schulson, E. M. (1982). The tensile strength of ice as a function of grain size. *Acta Metallurgica*, *30*(8), 1511–1514. https://doi.org/10.1016/0001-6160(82)90171-7

De Achaval, E. M., Nasello, O. B., & Ceppi, E. A. (1987). Grain growth in laboratory prepared ice: Solute effects. *Le Journal de Physique Colloques*, *48*(C1), C1-283-C1-288. https://doi.org/10.1051/jphyscol:1987140

De Bresser, J. H. P., Peach, C. J., Reijs, J. P. J., & Spiers, C. J. (1998). On dynamic recrystallization during solid state flow: Effects of stress and temperature. *Geophysical Research Letters*, *25*(18), 3457–3460. https://doi.org/10.1029/98GL02690

Evans, B., & Dresen, G. (1991). *Deformation of Earth Materials: Six Easy Pieces*. https://doi.org/10.1002/rog.1991.29.s2.823

Fan, S., Prior, D. J., Pooley, B., Bowman, H., Davidson, L., Wallis, D., Piazolo, S., Qi, C., Goldsby, D. L., & Hager, T. F. (2023). Grain growth of natural and synthetic ice at 0°C. *The Cryosphere*, *17*(8), 3443–3459. https://doi.org/10.5194/tc-17-3443-2023

Faria, S. H., Weikusat, I., & Azuma, N. (2014a). The microstructure of polar ice. Part I: Highlights from ice core research. *Journal of Structural Geology*, *61*, 2–20. https://doi.org/10.1016/j.jsg.2013.09.010

Faria, S. H., Weikusat, I., & Azuma, N. (2014b). The microstructure of polar ice. Part II: State of the art. *Journal of Structural Geology*, *61*, 21–49. https://doi.org/10.1016/j.jsg.2013.11.003

Gleiter, H. (1969). Theory of grain boundary migration rate. *Acta Metallurgica*, *17*(7), 853–862. https://doi.org/10.1016/0001-6160(69)90105-9

Goldsby, D. L., & Kohlstedt, D. L. (1997). Grain boundary sliding in fine-grained Ice I. *Scripta Materialia*, *37*(9), 1399–1406. https://doi.org/10.1016/S1359-6462(97)00246-7

Goldsby, D. L., & Kohlstedt, D. L. (2001). Superplastic deformation of ice: Experimental observations. *Journal of Geophysical Research: Solid Earth*, *106*(B6), 11017–11030. https://doi.org/10.1029/2000JB900336

https://doi.org/10.5194/egusphere-2025-6040
Preprint. Discussion started: 10 December 2025

Grinsted, A., Rathmann, N. M., Mottram, R., Solgaard, A. M., Mathiesen, J., & Hvidberg, C. S. (2024). Failure strength of glacier ice inferred from Greenland crevasses. *The Cryosphere*, *18*(4), 1947–1957. https://doi.org/10.5194/tc-18-1947-2024

Hier-Majumder, S., & Abbott, M. E. (2010). Influence of dihedral angle on the seismic velocities in partially molten rocks. *Earth and Planetary Science Letters*, *299*(1), 23–32. https://doi.org/10.1016/j.epsl.2010.08.007

Holness, M. B., Cheadle, M. J., & McKenzie, D. (2005). On the Use of Changes in Dihedral Angle to Decode Late-stage Textural Evolution in Cumulates. *Journal of Petrology*, *46*(8), 1565–1583. https://doi.org/10.1093/petrology/egi026

Holness, M. B., Humphreys, M. C. S., Sides, R., Helz, R. T., & Tegner, C. (2012). Toward an understanding of disequilibrium dihedral angles in mafic rocks. *Journal of Geophysical Research: Solid Earth*, *117*(B6). https://doi.org/10.1029/2011JB008902

Jellinek, H. H. G., & Gouda, V. K. (1969). Grain Growth in Polycrystalline Ice. *Physica Status Solidi (b)*, *31*(1), 413–423. https://doi.org/10.1002/pssb.19690310149

Ketcham, W. M., & Hobbs, P. V. (1969). An experimental determination of the surface energies of ice. *The Philosophical Magazine: A Journal of Theoretical Experimental and Applied Physics*, *19*(162), 1161–1173. https://doi.org/10.1080/14786436908228641

Kihoulou, M., Choblet, G., Tobie, G., Kalousová, K., & Čadek, O. (2025). *Grain size evolution and heat transfer regime in the shells of icy moons* (No. EPSC-DPS2025-1519). EPSC-DPS2025. Copernicus Meetings. https://doi.org/10.5194/epsc-dps2025-1519

King, M. D., Howat, I. M., Jeong, S., Noh, M. J., Wouters, B., Noël, B., & van den Broeke, M. R. (2018). Seasonal to decadal variability in ice discharge from the Greenland Ice Sheet. *The Cryosphere*, *12*(12), 3813–3825. https://doi.org/10.5194/tc-12-3813-2018

Kingslake, J., Skarbek, R., Case, E., & McCarthy, C. (2022). Grain-size evolution controls the accumulation dependence of modelled firn thickness. *The Cryosphere*, *16*(9), 3413–3430. https://doi.org/10.5194/tc-16-3413-2022

Kulessa, B., Booth, A. D., O'Leary, M., McGrath, D., King, E. C., Luckman, A. J., Holland, P. R., Jansen, D., Bevan, S. L., Thompson, S. S., & Hubbard, B. (2019). Seawater softening of suture zones inhibits fracture propagation in Antarctic ice shelves. *Nature Communications*, *10*(1), 5491. https://doi.org/10.1038/s41467-019-13539-x

https://doi.org/10.5194/egusphere-2025-6040
Preprint. Discussion started: 10 December 2025

Lee, R. W., & Schulson, E. M. (1988). The Strength and Ductility of Ice Under Tension. *Journal of Offshore Mechanics and Arctic Engineering*, *110*(2), 187–191. https://doi.org/10.1115/1.3257049

Litwin, K. L., Zygielbaum, B. R., Polito, P. J., Sklar, L. S., & Collins, G. C. (2012). Influence of temperature, composition, and grain size on the tensile failure of water ice: Implications for erosion on Titan. *Journal of Geophysical Research: Planets*, *117*(E8). https://doi.org/10.1029/2012JE004101

McCarthy, C., Nielson, M. A., Coonin, A. N., Minker, J. S., & Domingos, A. A. (2019). Acoustic and Microstructural Properties of Partially Molten Samples in the Ice–Ammonia System. *Geosciences*, *9*(8), Article 8. https://doi.org/10.3390/geosciences9080327

Nasello, O. B., Di Prinzio, C. L., & Guzmán, P. G. (2007). Grain boundary properties of ice doped with small concentrations of potassium chloride (KCl). *Journal of Physics: Condensed Matter*, *19*(24), 246218. https://doi.org/10.1088/0953-8984/19/24/246218

Nimmo, F. (2025). Surfaces, interiors and evolution of solar system moons. *Proceedings of the Royal Society A: Mathematical, Physical and Engineering Sciences*, *481*(2312), 20240806. https://doi.org/10.1098/rspa.2024.0806

Nimmo, F., & Manga, M. (Eds.). (2017). Geodynamics of Europa's Icy Shell. In *Europa*. University of Arizona Press. https://doi.org/10.2307/j.ctt1xp3wdw

Petrovic, J. J. (2003). Review Mechanical properties of ice and snow. *Journal of Materials Science*, *38*(1), 1–6. https://doi.org/10.1023/A:1021134128038

Poirier, J. P., Boloh, L., & Chambon, P. (1983). Tidal dissipation in small viscoelastic ice moons: The case of Enceladus. *Icarus*, *55*(2), 218–230. https://doi.org/10.1016/0019-1035(83)90076-3

Ranganathan, M., & Minchew, B. (2024). A modified viscous flow law for natural glacier ice: Scaling from laboratories to ice sheets. *Proceedings of the National Academy of Sciences*, *121*(23), e2309788121. https://doi.org/10.1073/pnas.2309788121

Ranganathan, M., & Robel, A. A. (2025). Evolution of Ice Tensile Strength With Grain Size: Implications for Future Mass Loss From Pine Island Glacier. *Geophysical Research Letters*, *52*(17), e2025GL117691. https://doi.org/10.1029/2025GL117691

Ravikumar, S., McCarthy, C., Singh, V., & Czernik, T. B. (2025). Binary Systems for Ocean Worlds: The Influence of Soluble Impurities on Ice Crystal Growth and Morphology. *Crystal Growth & Design*, acs.cgd.4c01353. https://doi.org/10.1021/acs.cgd.4c01353

https://doi.org/10.5194/egusphere-2025-6040
Preprint. Discussion started: 10 December 2025

Rignot, E., Mouginot, J., & Scheuchl, B. (2011). Ice Flow of the Antarctic Ice Sheet. *Science*, *333*(6048), 1427–1430. https://doi.org/10.1126/science.1208336

Roessiger, J., Bons, P. D., Griera, A., Jessell, M. W., Evans, L., Montagnat, M., Kipfstuhl, S., Faria, S. H., & Weikusat, I. (2011). Competition between grain growth and grain-size reduction in polar ice. *Journal of Glaciology*, *57*(205), 942–948. https://doi.org/10.3189/002214311798043690

Schohn, C. M., Iverson, N. R., Zoet, L. K., Fowler, J. R., & Morgan-Witts, N. (2025). Linear-viscous flow of temperate ice. *Science*, *387*(6730), 182–185. https://doi.org/10.1126/science.adp7708

Schulson, E. M., Lim, P. N., & Lee, R. W. (1984). A brittle to ductile transition in ice under tension. *Philosophical Magazine A*, *49*(3), 353–363. https://doi.org/10.1080/01418618408233279

Seltzer, C. (2025). *[DATASET] Supplementary data for "Saltwater exposure accelerates ice grain growth and increases fracture vulnerability"* [Dataset]. Zenodo. https://doi.org/10.5281/zenodo.17602183

Steinbrügge, G., Voigt, J. R. C., Wolfenbarger, N. S., Hamilton, C. W., Soderlund, K. M., Young, D. A., Blankenship, D. D., Vance, S. D., & Schroeder, D. M. (2020). Brine Migration and Impact-Induced Cryovolcanism on Europa. *Geophysical Research Letters*, *47*(21), e2020GL090797. https://doi.org/10.1029/2020GL090797

Suganuma, Y., Itaki, T., Haneda, Y., Kusahara, K., Obase, T., Ishiwa, T., Omori, T., Ikehara, M., McKay, R., Seki, O., Hirano, D., Fujii, M., Kato, Y., Amano, A., Tokuda, Y., Iwatani, H., Suzuki, Y., Hirabayashi, M., Matsuzaki, H., … Miura, H. (2025). Antarctic ice-shelf collapse in Holocene driven by meltwater release feedbacks. *Nature Geoscience*, 1–8. https://doi.org/10.1038/s41561-025-01829-7

Ultee, L., Meyer, C., & Minchew, B. (2020). Tensile strength of glacial ice deduced from observations of the 2015 eastern Skaftá cauldron collapse, Vatnajökull ice cap, Iceland. *Journal of Glaciology*, *66*(260), 1024–1033. https://doi.org/10.1017/jog.2020.65

Vaughan, D. G. (1993). Relating the occurrence of crevasses to surface strain rates. *Journal of Glaciology*, *39*(132), 255–266. https://doi.org/10.3189/S0022143000015926

Wang, Q., Fan, S., & Qi, C. (2024). Grain growth of ice doped with soluble impurities. *The Cryosphere*, *18*(3), 1053–1084. https://doi.org/10.5194/tc-18-1053-2024

Weeks, W. (2010). *On Sea Ice*. University of Alaska Press.

https://doi.org/10.5194/egusphere-2025-6040
Preprint. Discussion started: 10 December 2025

Wells-Moran, S., Ranganathan, M., & Minchew, B. (2025). Fracture criteria and tensile strength for natural glacier ice calibrated from remote sensing observations of Antarctic ice shelves. *Journal of Glaciology*, *71*, e47. https://doi.org/10.1017/jog.2024.104

Wolfenbarger, N. S., Fox-Powell, M. G., Buffo, J. J., Soderlund, K. M., & Blankenship, D. D. (2022). Compositional Controls on the Distribution of Brine in Europa's Ice Shell. *Journal of Geophysical Research: Planets*, *127*(9), e2022JE007305. https://doi.org/10.1029/2022JE007305

Xu, Z., Hefferan, C. M., Li, S. F., Lind, J., Suter, R. M., Abdeljawad, F., & Rohrer, G. S. (2023). Energy dissipation by grain boundary replacement during grain growth. *Scripta Materialia*, *230*, 115405. https://doi.org/10.1016/j.scriptamat.2023.115405

Yamauchi, H., McCarthy, C., Leeman, J. R., & Holtzman, B. K. (2024). A cryogenic forced oscillation apparatus to measure anelasticity of ice. *Review of Scientific Instruments*, *95*(7), 075108. https://doi.org/10.1063/5.0185885

Yamauchi, H., & Takei, Y. (2024). Effect of Melt on Polycrystal Anelasticity. *Journal of Geophysical Research: Solid Earth*, *129*(4), e2023JB027738. https://doi.org/10.1029/2023JB027738